Paddle-Wheel Shaped Copper(II)-Adenine Discrete Entities As Supramolecular Building Blocks To Afford Porous Supramolecular Metal-Organic Frameworks (SMOFs)

ARTICLE *in* CRYSTAL GROWTH & DESIGN · AUGUST 2014

Impact Factor: 4.89 · DOI: 10.1021/cg500634y

8 AUTHORS, INCLUDING:

Garikoitz Beobide
Universidad del País Vasco / Euskal Herriko U…
54 PUBLICATIONS **715** CITATIONS
SEE PROFILE

Oscar Castillo
Universidad del País Vasco / Euskal Herriko U…
133 PUBLICATIONS **1,972** CITATIONS
SEE PROFILE

Michael Fröba
University of Hamburg
219 PUBLICATIONS **5,749** CITATIONS
SEE PROFILE

Pascual Roman
Universidad del País Vasco / Euskal Herriko U…
192 PUBLICATIONS **3,066** CITATIONS
SEE PROFILE

CRYSTAL GROWTH & DESIGN

Article

pubs.acs.org/crystal

Paddle-Wheel Shaped Copper(II)-Adenine Discrete Entities As Supramolecular Building Blocks To Afford Porous Supramolecular Metal–Organic Frameworks (SMOFs)

Jintha Thomas-Gipson,[†] Garikoitz Beobide,*[,†] Oscar Castillo,*[,†] Michael Fröba,[‡] Frank Hoffmann,[‡] Antonio Luque,[†] Sonia Pérez-Yáñez,[†] and Pascual Román[†]

[†]Departamento de Química Inorgánica, Facultad de Ciencia y Tecnología, Universidad del País Vasco (UPV/EHU), Apartado 644, E–48080 Bilbao, Spain

[‡]Institute of Inorganic and Applied Chemistry, Department of Chemistry, University of Hamburg, Martin-Luther-King-Platz 6, D-20146 Hamburg, Germany

Supporting Information

ABSTRACT: The present work assesses the ability of $[Cu_2(\mu\text{-adenine})_4(X)_2]^{2+}$ and $[Cu_2(\mu\text{-adenine})_2(\mu\text{-X})_2(X)_2]$ (X: Cl^- or Br^-) metal-nucleobase dinuclear entities to build up supramolecular metal–organic frameworks (SupraMOFs) based on the complementary hydrogen bonding interactions established by the Watson–Crick and Hoogsteen faces of adjacent adenine moieties. The noncoplanar disposition of these synthons in the $[Cu_2(\mu\text{-adenine})_4(X)_2]^{2+}$ building unit leads to an open framework with one-dimensional (1D) channels of ca. 6 Å in compounds $[Cu_2(\mu\text{-adenine})_4(Cl)_2]\text{-}Cl2\cdot\sim 2MeOH$ (**1**, **SMOF-1**) and $[Cu_2(\mu\text{-adenine})_4(Br)_2]\text{-}Br_2\cdot\sim 2$ MeOH (**2**, **SMOF-2**) sustained through the hydrogen bonding base pairing interactions among the Watson–Crick faces. In the case of the second building unit, $[Cu_2(\mu\text{-adenine})_2(\mu\text{-X})_2(X)_2]$, the coplanar arrangement of the two adenines in the dimeric unit does not allow a three-dimensional (3D) supramolecular architecture based only on the complementary hydrogen bonding interactions between the nucleobases. Therefore, other supramolecular interactions involving the halide ions and solvent molecules are crucial for determining the features of the crystal packing. In compound $[Cu_2(\mu\text{-adenine})_2(\mu\text{-Cl})_2(Cl)_2]\cdot 2MeOH$ (**3**, **SMOF-3**), base pairing interactions between adjacent adenines produce 1D supramolecular ribbons of dinuclear entities. These ribbons establish additional hydrogen bonds between the Hoogsteen face and the chloride anions of adjacent ribbons that are also reinforced by the presence of π–π stacking interactions among the adenines leading to a rigid synthon that gives rise to a robust 3D skeleton with the presence of micropores occupied by solvent molecules. In the case of the bromide analogue, the weaker hydrogen acceptor capacity of the bromide allows the solvent molecules to disrupt the self-assembly process of the dinuclear entities and prevents the formation of an open-framework supramolecular structure leading to the nonporous $[Cu_2(\mu\text{-adenine})_2(\mu\text{-Br})_2(Br)_2]\cdot 2PrOH$ (**4**) compound. According to gas adsorption studies, **SMOF-1**, **SMOF-2**, and **SMOF-3** present a surface instability that creates a diffusion barrier that can be permeated only by strong interacting adsorbate molecules with high kinetic energy such as CO_2 but not N_2, H_2, and CH_4. This feature makes them attractive for selective gas adsorption and separation technologies.

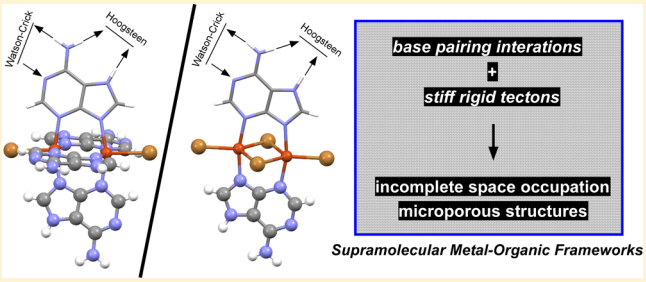

INTRODUCTION

The coordination chemistry of metal ion interactions with purine nucleobases has attracted enormous attention because of its biological relevance, structural diversity, molecular recognition behaviors, and potential applications as advanced functional materials.[1] Adenine (6-aminopurine) has a wide range of binding possibilities through the endocyclic N9, N7, N3, N1, and exocyclic N6 nitrogen atoms as donor sites[2] resulting in a vast number of products. Moreover, when a metal–adenine complex is formed, the noncoordinated nitrogen donor sites confer the ability to establish a wide variety of hydrogen bonding based supramolecular interactions.[3] On the other hand, the purine ligands are well-known for their ability to build dinuclear complexes by means of the N3 and N9 bridging mode,[4] and previous works have demonstrated that either adenine or adeninate ligands tend to form paddle-wheel shaped dinuclear complexes, such as $[Cu_2(\mu\text{-adenine})_4]^{4+}$, $[Cu_2(\mu\text{-adeninato})_4]$, or $[Cu_2(\mu\text{-adeninato})_2(X)_2]$ (where X: $RCOO^-$, halide···).[5] These entities can self-assemble by means of the well-known base pairing of the Watson–Crick (N6–H, N1) and Hoogsteen faces (N6–H, N7) and by π–π stacking interactions. Nonetheless, additional factors present in the

Received: May 2, 2014
Revised: June 11, 2014
Published: June 13, 2014

Scheme 1

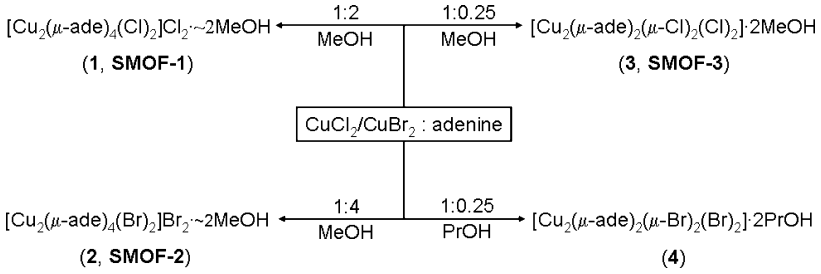

reaction media, such as interactions with solvent molecules or counterions, can disrupt the direct hydrogen bonding interactions between the nucleobases.[6]

On the basis of these facts, we have designed a synthetic strategy to develop rigid supramolecular open-networks showing permanent microporosity as an alternative to more conventional metal−organic frameworks (MOFs).[7] It deserves mentioning that examples of microporous compounds whose crystal structure is sustained by noncovalent interactions are scarce, mainly due to the difficulties inherent to the design of such systems and the usually assumed weakeness of the supramolecular connectivity.[8] Our approach is based on employing as supramolecular building blocks discrete metal−adenine complexes in which two or more nucleobases are tightly anchored to the metal centers by at least two donor positions (N3, N9 sites of the adenine in the present case). This coordination motif imposes a rigid structure to the building unit that is a key factor of our crystal design. In addition, the geometrical arrangement of the nucleobases around the metal centers is otherwise difficult to achieve for other systems such as organic molecules functionalized with adenine residues. In these discrete complexes, as many hydrogen donor/acceptor positions of the nucleobase remain free, the entities are able to self-assemble among them by means of rigid double or triple complementary hydrogen bonds. Due to the geometric restraints of the H-bonding synthons and of the metal-nucleobase complex itself, an efficient packing of the supramolecular building units is hindered allowing the presence of a large empty volume: an open-framework supramolecular crystal building. The voids will be usually occupied by solvent molecules, and as consequence, in order to achieve a compound with permanent porosity, the scheme of supramolecular interactions established among the metal-nucleobase entities must be strong enough to avoid the collapse of the crystal structure when the solvent is evacuated. This fact is the reason to select metal-nucleobase systems. The nucleobases self-recognize by double or triple hydrogen bonding ensuring a superior strength of the resulting supramolecular crystal building. The pioneering example that makes use of this strategy to provide a molecular porous material with formula $[Cu_2(\mu\text{-adenine})_4Cl_2]Cl_2$ was published by us in 2011.[9] Later, Zaworotko et al. reported an analogous compound replacing the chlorides by bulkier TiF_6^{2-} anions improving the chemical stability of the supramolecular network toward humidity.[10]

In this work we assess the ability of two types of metal-nucleobase dinuclear entities $[Cu_2(\mu\text{-adenine})_4(X)_2]^{2+}$ and $[Cu_2(\mu\text{-adenine})_2(\mu\text{-X})_2(X)_2]$ (where X: Cl^- or Br^-) to build up supramolecular metal−organic frameworks (SMOFs) based on base pairing interactions between either Watson−Crick faces or Hoogsteen faces. The control over the molecular structure of the dinuclear entities is easily achieved by means of the copper(II) halide/adenine ratio. As a result of the non-coplanarity of the adenines in $[Cu_2(\mu\text{-adenine})_4(X)_2]^{2+}$ entities, the base pairing sustained self-assembling process yields an open framework with one-dimensional (1D) channels occupied by methanol solvent molecules: $[Cu_2(\mu\text{-adenine})_4(Cl)_2]Cl_2\cdot\sim$2MeOH (**1**, **SMOF-1**) and $[Cu_2(\mu\text{-adenine})_4(Br)_2]Br_2\cdot\sim$2MeOH (**2**, **SMOF-2**). Regarding $[Cu_2(\mu\text{-adenine})_2(\mu\text{-X})_2(X)_2]$ dinuclear entity, compounds $[Cu_2(\mu\text{-adenine})_2(\mu\text{-Cl})_2(Cl)_2]\cdot$2MeOH (**3**, **SMOF-3**) and $[Cu_2(\mu\text{-adenine})_2(\mu\text{-Br})_2(Br)_2]\cdot$2PrOH (**4**) were yielded. In the latter cases, the coplanar arrangement of the adenines reduces the dimensionality of the supramolecular polymer obtained from the base pairing interactions. As a consequence, the coordinated halides and solvent molecules play a crucial role stabilizing the overall three-dimensional (3D) crystal structure. In the case of the chloride-based compound **3** (**SMOF-3**), the combination of base pairing, $\pi-\pi$ stacking, and additional hydrogen bonding interactions involving the chloride anions provides a rigid scheme of supramolecular interactions that precludes an efficient occupation of the space leading to a robust open-framework supramolecular structure. The weaker nature of the hydrogen bonds involving bromide anions allows the solvent molecules to disrupt the previously described supramolecular interaction scheme leading to nonporous compound **4**. Even though previously reported N_2 adsorption experiments performed on samples of $[Cu_2(\mu\text{-adenine})_4(Cl)_2]Cl_2$ (**SMOF-1**)[11] did not show significant adsorption, the present work will prove the permanent porosity of **SMOF-1**, **SMOF-2**, and **SMOF-3** compounds by means of CO_2 adsorption isotherms at 273 K. The different adsorption behavior is attributed to a surface instability, because of the air humidity, that creates a diffusion barrier that only can be permeated by well-suited adsorbates under specific adsorption conditions. Therefore, these compounds can be envisaged as potential materials for selective gas adsorption or separation purposes.

EXPERIMENTAL SECTION

Synthesis. All the chemicals were of reagent grade and were used as commercially obtained. The purity of the synthesized samples was checked by means of powder X-ray diffraction, along with the elemental and thermogravimetric analyses. Scheme 1 describes the most notorious synthesis conditions to afford compounds **1**−**4**.

$[Cu_2(\mu\text{-adenine})_4Br_2]Br_2\sim$2MeOH (2, SMOF-2). A total of 0.0112 g of cupric bromide (0.05 mmol) dissolved in 5 mL of methanol was added dropwise to the hot stirring solution of 0.0273 g of adenine (0.2 mmol) dissolved in 30 mL of methanol at 50 °C. Immediately after the reagents were mixed, compound **2** precipitated as a blue polycrystalline product. Yield: 90%. Anal. Calcd (found) for $C_{22}H_{28}Br_4Cu_2N_{20}O_2$: C, 25.13 (25.24); H, 2.68 (2.81); N, 26.65 (26.53); Cu, 12.09 (11.97). IR (KBr, cm^{-1}): 3330s, 3170s, 1650vs, 1515w, 1460m, 1348w, 1320m, 1260w, 1215m, 1182w, 1148w,

dx.doi.org/10.1021/cg500634y | Cryst. Growth Des. 2014, 14, 4019−4029

Table 1. Single-Crystal Data and Structural Refinement Details of Compounds 2, 3, and 4

compound	2	3	4
formula	$C_{22}H_{28}Br_4Cu_2N_{20}O_2$	$C_{12}H_{18}Cl_4Cu_2N_{10}O_2$	$C_{16}H_{26}Br_4Cu_2N_{10}O_2$
MW [g mol^{-1}]	1051.36	603.24	837.19
crystal system	trigonal	monoclinic	monoclinic
space group	$R\bar{3}m$	$C2/c$	$P2_1/c$
a [Å]	27.1979(9)	22.2245(18)	9.1344(7)
b [Å]	27.1979(9)	13.8069(10)	11.0778(10)
c [Å]	15.4999(4)	7.0204(6)	13.0778(11)
α [°]	90	90	90
β [°]	90	108.280(6)	103.873(7)
γ [°]	120	90	90
V [Å^3]	9929.6(5)	2045.5(3)	1284.7(2)
Z	9	4	2
ρ_{calcd} (g·cm^{-3})	1.582	1.959	2.164
μ (mm^{-1})	4.630	2.636	7.912
reflections collected	31767	9439	18741
unique data/parameters	2837/109	9439/127	3059/161
R_{int}	0.0465	0.0695	0.0942
goodness of fit (S)[a]	1.234	1.089	1.119
R_1[b]/wR_2[c] [$I > 2\sigma(I)$]	0.0927/0.2997	0.0778/0.2048	0.0504/0.0927
R_1[b]/wR_2[c] [all data]	0.1112/0.3107	0.1119/0.2342	0.0688/0.1005

[a] $S = [\sum w(F_0^2 - F_c^2)^2/(N_{obs} - N_{param})]^{1/2}$. [b] $R_1 = \sum||F_0| - |F_c||/\sum|F_0|$. [c] $wR_2 = [\sum w(F_0^2 - F_c^2)^2/\sum w|F_0|^2]^{1/2}$; $w = 1/[\sigma^2(F_0^2) + (aP)^2 + bP]$ where $P = (\max(F_0^2,0) + 2Fc^2)/3$ with a = 0.2000 (**2**), 0.1437 (**3**), 0.0235 (**4**), and b = 9.0683 (**4**).

1117m, 1022w, 970w, 934w(sh), 922w(sh), 790m, 738m, 683w, 610w, 563w, 545m. Crystals suitable for single crystal X-ray diffraction studies were grown by using the slow diffusion of a methanolic solution (12 mL) of adenine (0.0111 g, 0.08 mmol) into a propanolic solution (12 mL) of cupric bromide (0.0088 g, 0.04 mmol). After 1 week, compound **2** crystallized as deep blue colored single crystals along with some poor quality red crystals of compound **4**.

[Cu$_2$(μ-adenine)$_4$Cl$_2$]Cl$_2$·~2MeOH (1, SMOF-1). Compound **1** was prepared following the synthetic method mentioned in one of our previous works.[11] A total of 0.0171 g of cupric chloride dihydrate (0.1 mmol) dissolved in 5 mL of methanol were added dropwise to a hot stirring solution (50 °C) of 0.0273 g of adenine (0.2 mmol) dissolved in 30 mL of methanol. A blue precipitate corresponding to compound **1** was formed immediately on the addition of the cupric chloride solution. Yield: 90%. Anal. Calcd (found) for $C_{22}H_{28}Cl_4Cu_2N_{20}O_2$: C, 30.25 (30.19); H, 3.23 (3.19); N, 32.07 (32.26); Cu, 14.55 (14.62). IR (KBr, cm^{-1}): 3360s; 3170s; 1650vs; 1515w; 1460m; 1400m; 1350w; 1320m; 1210m; 1110w; 785w; 740w; 550m.

[Cu$_2$(μ-adenine)$_2$(μ-Cl)$_2$(Cl)$_2$]·2MeOH (3, SMOF-3). A total of 0.0682 g of cupric chloride dihydrate (0.4 mmol) dissolved in 10 mL of methanol were added dropwise to a hot stirring solution (50 °C) of 0.0136 g of adenine (0.1 mmol) dissolved in 20 mL of methanol and stirred for half an hour. After the reagents were mixed, compound **3** appeared as a green precipitate. Yield: 95%. Anal. Calcd (found) for $C_{12}H_{18}Cl_4Cu_2N_{10}O_2$: C, 23.89 (23.92); H, 3.01 (3.14); N, 23.22 (23.18); Cu, 21.07 (21.03). IR (KBr, cm^{-1}): 3387s, 3142s(sh), 3103s(sh), 1666vs, 1611m, 1580m, 1520m, 1478m, 1450s, 1404vs, 1383w, 1356w(sh), 1347w(sh), 1318vs, 1262w, 1244w, 1215m, 1291w, 1170m, 1111vs, 1016w, 976w(sh), 970w(sh), 931m, 788m, 737m(sh), 722m(sh), 680m, 633w, 597m, 573w, 548s. Single crystals were obtained by slow diffusion of a methanolic solution (10 mL) 0.0171 g of cupric chloride (0.1 mmol) into another methanolic solution (30 mL) containing 0.0277 g of adenine (0.2 mmol) and 16.9 μL of concentrated hydrochloric acid (37%). Green-colored single crystals of compound **3** were formed along with blue colored crystals of compound **1**.

[Cu$_2$(μ-adenine)$_2$(μ-Br)$_2$(Br)$_2$]·2PrOH (4). A hot propanolic solution (40 mL, 50 °C) of 0.0136 g of adenine (0.1 mmol) was added dropwise to a second propanolic solution (10 mL) of 0.0893 g of cupric bromide (0.4 mmol). Immediately, an unidentified brown precipitate appears. The reaction mixture was left stirring for half an hour. Afterward the precipitate is collected by filtration, and the mother-liquid solution is left evaporating at room conditions. One month later, red crystals of compound **4** are obtained. Yield: 20%. Anal. Calcd (found) for $C_{16}H_{26}Br_4Cu_2N_{10}O_2$: C, 22.96 (22.91); H, 3.13 (3.09); N, 16.73 (16.78); Cu, 15.18 (15.15). IR (KBr, cm^{-1}): 3380s, 3226s,3293s, 3240s, 3193s, 3130s, 2953s, 1666vs, 1612m, 1476w, 1460w, 1405m, 1384w, 1357w, 1344w, 1320s, 1262w, 1220m, 1175w, 1112m, 1050w, 1002s, 972w, 930w, 875m, 802w, 876m, 736m, 711w, 677w, 663w, 613m, 569m, 538w, 472w, 463w.

Physical Measurements. Elemental analyses (C, H, N) were performed on an Euro EA elemental analyzer, whereas the metal content was determined by inductively coupled plasma atomic emission spectrometer (ICP-AES) from Horiba Yobin Yvon Activa. The IR spectra (KBr pellets) were recorded on a FTIR 8400S Shimadzu spectrometer in the 4000−400 cm^{-1} spectral region. Thermal analyses (TG/DTA) were performed on a TA Instruments SDT 2960 thermal analyzer in a synthetic air atmosphere (79% N_2/21% O_2) with a heating rate of 5 °C·min^{-1}. Prior to gas adsorption measurements all samples were activated in vacuum at 100−180 °C for 6−24 h. Lower and greater activation temperatures did not result in samples with higher gas uptake capacity. The powder X-ray diffraction patterns on the outgassed samples showed that the structure remains stable without loss of crystallinity. Nitrogen physisorption data were recorded with a Quantachrome QUADRASORB-SI-MP at 77 K. The specific surface area was calculated from the adsorption branch in the relative pressure interval from 0.01 to 0.10 using the Brunauer−Emmett−Teller (BET) method. Volumetric carbon dioxide and hydrogen physisorption data were recorded at 273 K on a Quantachrome Autosorb-iQ-MP and at 77 K on a Quantachrome Autosorb-1C (purity of hydrogen: 99.999%).

X-ray Diffraction Data Collection and Structure Determination. The single crystal X-ray diffraction data collections were done at 293(2) K for compound **2** and at 100(2) K for compounds **3** and **4** on an Oxford Diffraction Xcalibur diffractometer with graphite-monochromated Mo−Kα radiation (λ = 0.71073 Å). The data reduction was done with the CrysAlisPro program.[12] All the structures were solved by direct methods using the SIR92 program[13] and refined by full-matrix least-squares on F^2 including all reflections (SHELXL97).[14] All calculations for these structures were performed using the WINGX crystallographic software package.[15] After the initial structure solution was completed, the difference Fourier map for

dx.doi.org/10.1021/cg500634y | Cryst. Growth Des. 2014, 14, 4019−4029

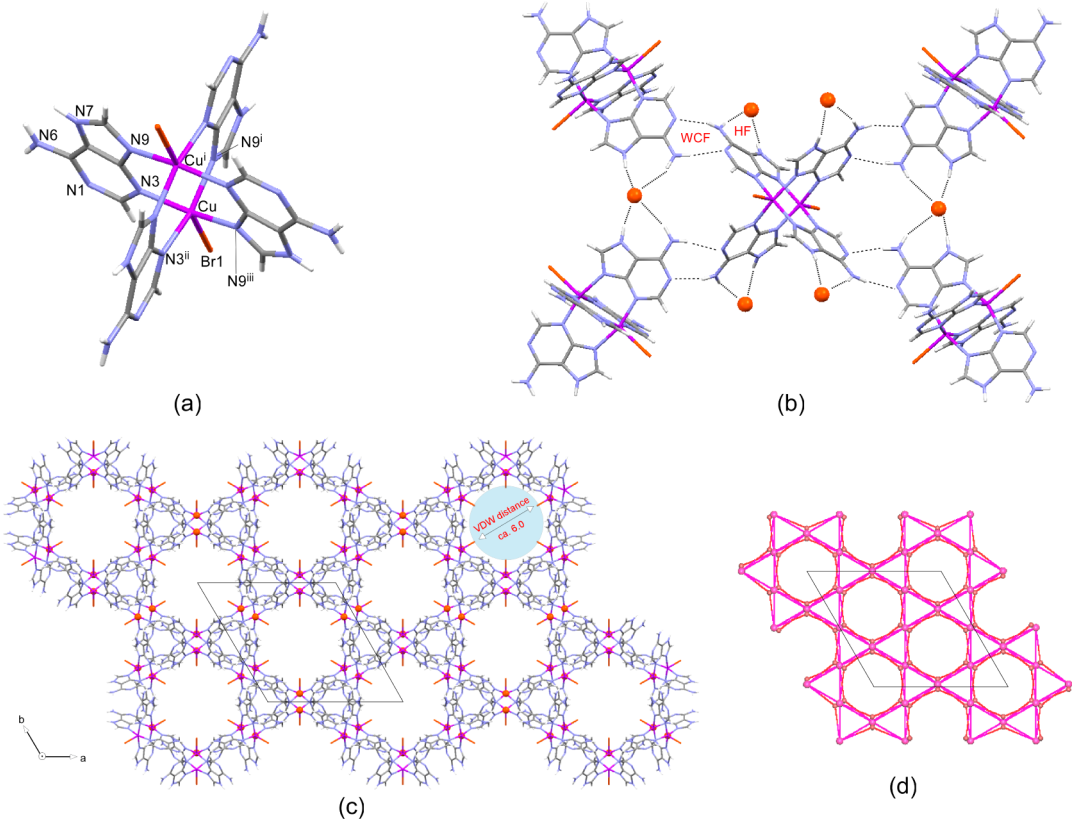

Figure 1. Crystal structure features of **SMOF-2**: (a) Structural units with the atomic numbering scheme. (b) Details of the adenine base pairing interaction through the Watson−Crick face (WCF) and of the Hoogsteen Face (HF) mediated adenine···bromide interaction (free bromide anions are represented as orange spheres). (c) Perspective view of the 3D framework along the *c*-axis showing the pores. Solvated methanol molecules are omitted for clarity. (d) Network topology.

Table 2. Selected Bond Lengths (Å) and Angles (deg) of Compounds 2, 3, and 4[a]

compound **2**			compound **3** (X = Cl)	compound **4** (X = Br)
Cu−N3	1.994(5)	Cu−N3^{i}	2.006(4)	1.963(5)
Cu−N9^{i}	2.016(6)	Cu−N9	1.983(4)	1.962(5)
Cu−Br1	3.080(2)	Cu−X1	2.241(1)	2.378(1)
		Cu−X2	2.342(1)	2.540(1)
		Cu−X2^{i}	2.757(1)	2.656(1)
Cu···Cu^{i}	3.082(1)	Cu···Cu^{i}	2.942(1)	2.902(1)
N3−Cu−N3^{ii}	88.1(3)	N3^{i}−Cu−N9	164.83(17)	165.8(2)
N3−Cu−N9^{i}	86.5(2)	N3^{i}−Cu−X1	96.71(13)	98.02(14)
N3−Cu−N9^{iii}	161.6(3)	N3^{i}−Cu−X2	87.19(14)	87.23(14)
N3−Cu−Br1	100.2(2)	N3^{i}−Cu−X2^{i}	83.77(13)	86.58(13)
N9^{i}−Cu−N9^{iii}	93.1(3)	N9−Cu−X1	94.32(13)	95.56(14)
N9^{i}−Cu−Br1	98.0(2)	N9−Cu−X2	87.19(14)	86.78(14)
		N9−Cu−X2^{i}	83.21(13)	83.73(14)
		X1-Cu−X2	144.00(6)	132.35(3)
		X1−Cu−X2^{i}	105.81(6)	115.45(3)
		X2−Cu−X2^{i}	110.07(4)	112.12(3)

[a]Symmetry codes. Compound **2**: (i) $x-y, -y, -z+2$; (ii) $-x+y+1, y, z$; (iii) $-x+1, -y, -z+2$. Compound **3**: (i) $-x+1/2, -y+1/2, -z+1$. Compound **4**: (i) $-x+1, -y, -z+2$.

compound **SMOF-2** showed the presence of substantial electron density at the voids of the crystal structure that was impossible to model. Therefore, its contribution was subtracted from the reflection data by the SQUEEZE method[16] as implemented in PLATON.[17] Crystal parameters and details of the final refinements of compounds **2**, **3**, and **4** are summarized in Table 1. The X-ray powder diffraction (PXRD) patterns for polycrystalline samples were collected on a Phillips X'PERT powder diffractometer with Cu−Kα radiation (λ = 1.54060 Å) over the range $5 < 2\theta < 70°$ with a step size of 0.02° and an acquisition time of 2 s per step at 20 °C.

RESULTS AND DISCUSSION

Structural Description of [Cu$_2$(μ-adenine)$_4$Br$_2$]Br$_2$·∼2MeOH (2, SMOF-2). This compound is isostructural to compound **1** (**SMOF-1**) whose crystal structure has been previously reported by us.[11] The crystal structure consists of

dx.doi.org/10.1021/cg500634y | *Cryst. Growth Des.* 2014, 14, 4019−4029

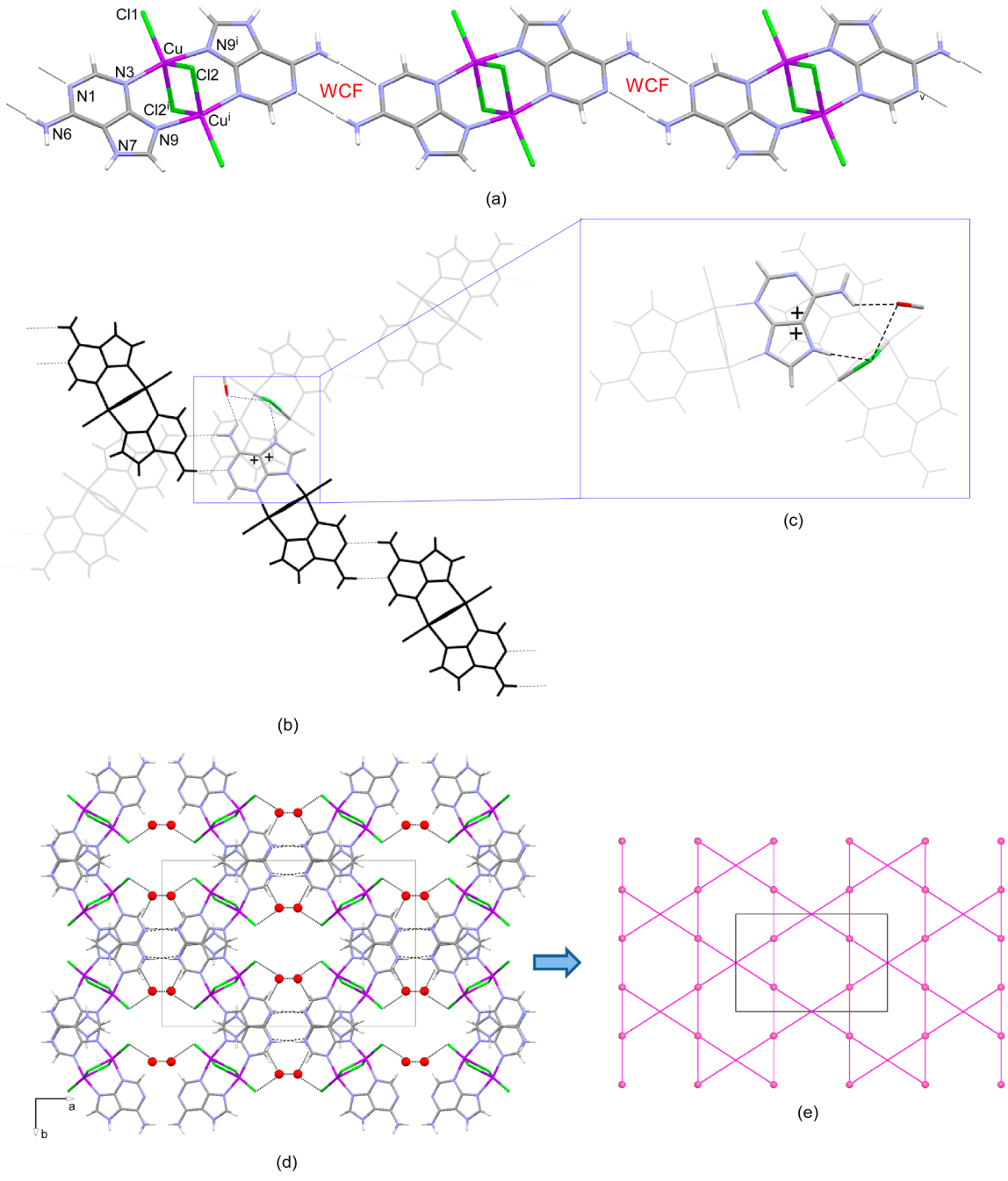

Figure 2. Crystal packing features in **SMOF-3**: (a) Strips of $[Cu_2(\mu\text{-adenine})_2(\mu\text{-Cl})_2Cl_2]$ dinuclear complexes grown by Watson−Crick base pairing interactions. (b, c) Dinuclear entities interacting through Cl···Hoogsteen face and $\pi-\pi$ interactions and the methanol hydrogen bonding mediating role. (d, e) View of the crystal packing along [1 0 0] direction and overall supramolecular conectivity. Dashed lines indicate hydrogen bonds, while double plus signals represent $\pi-\pi$ interactions.

paddle-wheel like $[Cu_2(\mu\text{-adenine})_4Br_2]^{2+}$ complexes, bromide counterions, and disordered methanol molecules. Figure 1 shows a perspective view of the dimeric entity together with the labeling scheme which is conventionally accepted for the adenine nucleobase for chemical and biological purposes, while coordination bonds and angles are gathered in Table 2. Four bridging adenine molecules are linked to the copper(II) atoms through their N3 and N9 nitrogen atoms to provide the core of the paddle-wheel shaped dinuclear entity. Two bromide anions occupy the apical positions resulting in an elongated square pyramidal coordination environment of the metal centers. The dimeric complex is sited on a 2/*m* crystallographic position and shows a UUDD conformation, referring the terms U(up) or D(down) to the coordination of each pyrimidinic N3 atoms to the upper or lower metal center.

The $[Cu_2(\mu\text{-adenine})_4Br_2]^{2+}$ dinuclear entities are cross-linked together by pairs of symmetry-related N6−H···N1 hydrogen bonding interactions between the Watson−Crick faces of two adjacent nucleobases to give a $R_2^2(8)$ ring. It deserves mentioning that this hydrogen bonding interaction scheme is a well-known structural synthon between self-assembling adenines.[5f,18] In the present compound the geometry and rigidity of the $[Cu_2(\mu\text{-adenine})_4Br_2]^{2+}$ entity (Figure 1) and the rigidity of the previously described hydrogen

dx.doi.org/10.1021/cg500634y | *Cryst. Growth Des.* 2014, 14, 4019−4029

bonding synthon make it suitable to assemble in such a way that it generates an open-supramolecular-framework because of the inefficient occupation of the space. This synthon involving the Watson−Crick faces yields by itself a four-connected uninodal 3D net with ***nbo*** topology and ($6^4.8^2$) point symbol (Figure 1d).[19] However, the cohesion of the structure is further strengthen by $R_2^1(7)$ type hydrogen bonding interaction established among the free bromide counterions and the Hoogsteen faces of two adenine of neighboring complexes. Considering both types of interactions (Watson−Crick base pairing and Hoogsteen···bromide) the supramolecular network can be alternatively described as an eight-connected uninodal with ***reo*** topology and ($3^8.4^8.5^8.6^4$) point symbol.

The resulting porous structure consists of 1D tubular channels that run along the crystallographic *c* axis with a diameter of 6.0 Å (distance among van der Waals surfaces of opposite chloride anions). These channels represent the 30% of crystal total volume,[20] and they are occupied by solvent methanol molecules in a highly disordered manner. Due to the greater size of bromide anion, these values are somewhat lower than those found in the chloride derivative (**SMOF-1**; pore diameter: 6.3 Å; accessible volume: 36%).

Structural Description of $[Cu_2(\mu\text{-adenine})_2(\mu\text{-Cl})_2(Cl)_2]\cdot 2MeOH$ (3, SMOF-3) and $[Cu_2(\mu\text{-adenine})_2(\mu\text{-Br})_2(Br)_2]\cdot 2PrOH$ (4). Both compounds are comprised of neutral centrosymmetric dimeric $[Cu_2(\mu\text{-adenine})_2(\mu\text{-X})_2(X)_2]$ entities (X: Cl^-, Br^-) (Figure 2). It shows some resemblances to the previously described $[Cu_2(\mu\text{-adenine})_4X_2]^{2+}$ dimeric entity of **SMOF-1** and **SMOF-2**. The overall paddle-wheel shape is retained, but two opposite adenine ligands have been replaced by two bridging halide anions giving rise to a neutral dimeric entity showing an UD conformation with regard to the adenine bridges and two capping halide anions. The intradimeric Cu···Cu distances (2.942(1) and 2.902(1) Å, for chloride and bromide analogues) are slightly shorter than that of **SMOF-1** and **-2** (3.064(1) and 3.082(1) Å). Each copper atom is pentacoordinated by a N_2X_3 donor set which resembles a compressed trigonal bipyramid. The equatorial plane consists of three halide atoms implying longer bond distances than the apical ones (Table 2) and X−Cu−X angles within the range of 106−144° and a deviation of ca. 0.05 Å for the Cu(II) atom. The apical positions are occupied by the N3 and N9 donor sites of two symmetry related adenine molecules with a N−Cu−N angle of ca. 165° and an angle between equatorial plane and Cu−N bond of 83−86°. The coordination bond distances of the bridging halide anions are slightly longer than those of the terminal one as usually happens.

Obviously, the coplanar arrangement of adenines in the dimeric $[Cu_2(\mu\text{-adenine})_2(\mu\text{-X})_2(X)_2]$ entity although does not preclude the polymerization through direct complementary hydrogen bonding interactions between the nucleobases reduces the dimensionality of the resulting supramolecular network. In the case of **SMOF-3**, the base pairing interaction between the Watson−Crick faces of $[Cu_2(\mu\text{-adenine})_2(\mu\text{-Cl})_2(Cl)_2]$ units gives rise to linear 1D supramolecular ribbons (Figure 2a) that spread along two different crystallographic directions [1 1 0] and [1 $\bar{1}$ 0]. These supramolecular ribbons are further cross-linked by means of both the hydrogen-bonding interactions between the Hoogsteen face and the bridging chloride and $\pi-\pi$ stacking interactions between adjacent adenines. The combination of the latter two types of interactions leads also to a relatively rigid synthon that extends the connectivity toward a robust supramolecular 3D one and, at the same time, precludes an efficient occupation of the space (Figure 2d). Considering both types of synthons (Watson−Crick base pairing and Hoogsteen···chloride/$\pi-\pi$ stacking) the supramolecular network can be described as a six-connected uninodal net with ***rob*** topology and ($4^8.6^6.8$) point symbol (Figure 2e). This packing generates 1D channels along the crystallographic *c* axis with an elliptical cross-section of ca. 5.5 × 7.5 Å, that are filled by solvation water molecules that represent a 21% of the total volume. Again, the combination of rigid metal-nucleobase building unit and geometrically restricted supramolecular synthons leads to an ineffective space occupation providing accessible space within the crystal structure of this material. It is worthy to mention that the hydrogen bonding interaction between the Hoogsteen side of the adenine and the chloride anion is reinforced by an indirect hydrogen bonded interaction mediated by a solvation methanol molecule that will involve, as it is discussed later, a relatively significant unit cell change upon the removal of the solvent molecules.

The weaker hydrogen bond acceptor nature of the bromide anion in comparison to chloride makes the crystal packing features of compound **4**, $[Cu_2(\mu\text{-adenine})_2(\mu\text{-Br})_2(Br)_2]\cdot 2PrOH$ (Figure 3), to be essentially different from that of its

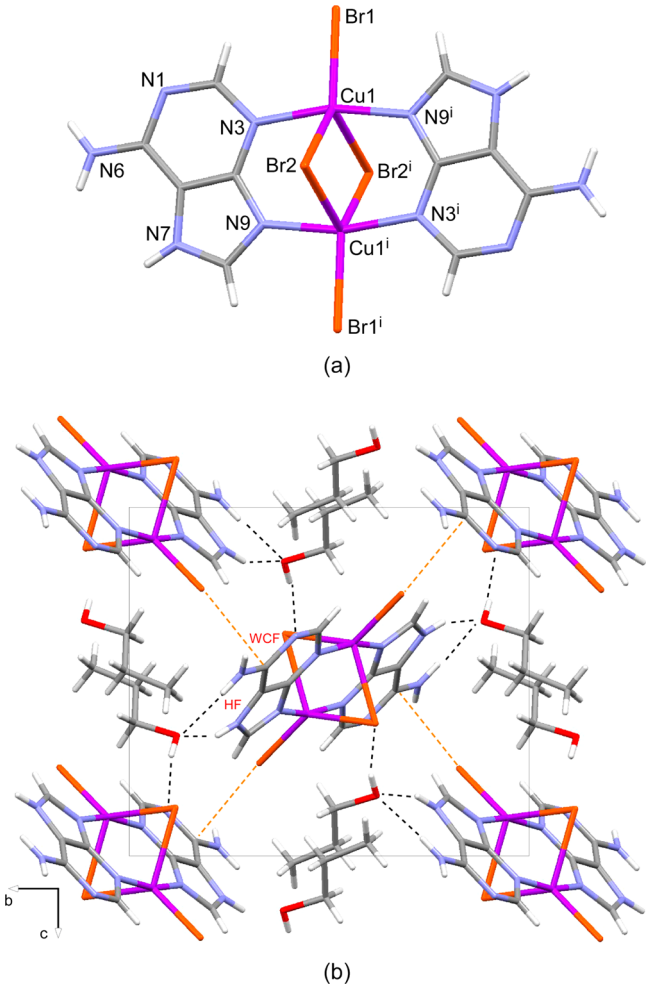

Figure 3. Dimeric unit (a) and view of the crystal packing along [1 0 0] direction (b) in compound **4**. Black dotted lines indicate hydrogen bonding interactions, while orange dashed lines indicate halide···π contacts.

dx.doi.org/10.1021/cg500634y | *Cryst. Growth Des.* 2014, 14, 4019−4029

chloride analogue (**SMOF-3**). It does not present base pairing interaction nor any other direct hydrogen bonding interaction between the adenine moieties and coordinated halides. In fact, the dinuclear entities are held together by the hydrogen bonding interactions mediated through the entrapped propan-1-ol molecules with the Hoogsteen and Watson−Crick faces of adjacent paddle-wheel entities. The Hoogsteen face of the nucleobase forms hydrogen bonding with the oxygen atom of the propan-1-ol molecule ($R_2^1(7)$ hydrogen bonded ring), while the Watson−Crick face of the adenine establishes a single hydrogen bond by means of the interaction of N1 with H atom of the alcohol group. The supramolecular interaction network of compound **4** is further reinforced by halide···π type interactions established between the terminal Br1 atoms and C6 carbon of the adenine (Br1···C6:3.489 Å). The lack of direct hydrogen bonding interactions among the rigid adenine moieties and the solvent mediated disruption of the hydrogen bonding network result in a nonporous crystal structure which collapses at temperatures close to 50 °C rendering an amorphous product, according to the thermogravimetric and variable temperature PXRD measurements.

Gas Adsorption Experiments on [Cu_2(μ-adenine)$_2$(Cl)$_2$]Cl_2·∼2MeOH (SMOF-1) and [Cu_2(μ-adenine)$_2$(Br)$_2$]Br_2·∼2MeOH (SMOF-2). Prior to gas adsorption experiments, thermal stability of both SMOFs was assessed by means of thermogravimetric and variable temperature PXRD experiments (see Supporting Information). According to the thermogravimetric data of both compounds, release of the solvent molecules hosted in the channels takes place between room temperature and 100 °C. In both cases the resulting compound remains stable up to 220 °C and the PXRD patterns at different temperatures (Figure 4a,b) do not differ substantially from that of the starting material, suggesting that the 3D open framework is retained after the removal of the methanol molecules. Above this temperature, it undergoes successive exothermic processes leading to CuO as final residue above 500 °C.

Freshly synthesized single crystals of **SMOF-1** and **-2** were used for gas adsorption experiments, and they were activated under a vacuum at temperatures ranging from 100 to 180 °C during 6−24 h to eliminate solvent guest molecules prior to measurements. Different outgassing conditions did not exert significant changes in N_2 uptake capacity. For clarity only the results of samples outgassed at 150 °C during 12 h are shown in subsequent figures. The adsorption curve collected at 77 K exhibits features resulting from multilayer adsorption. The fitting of the adsorption area to BET equation leads to surface area values of 26 and 14 m^2/g, respectively. These values are substantially smaller than the surface area calculated from the BET fittings on GCMC simulated N_2 adsorption isotherms (767 and 654 m^2/g, respectively), see details at the Supporting Information. Thereafter, H_2 adsorption experiments were also carried out by collecting isotherms at 77 K. Similarly to N_2, a negligible adsorption is observed for both compounds. A common explanation to such a difference between the experimental and expected porosity includes incomplete solvent removal, crystal collapse, or a massive presence of impurities. However, the weight loss of the outgassed sample fits the one expected from the compound formula, which suggests a quantitative removal of the solvent. The PXRD data confirms that the outgassed sample retains its crystallinity and, therefore, its bulk porous framework. Finally, the comparison of PXRD patterns, chemical analysis, and scanning electron

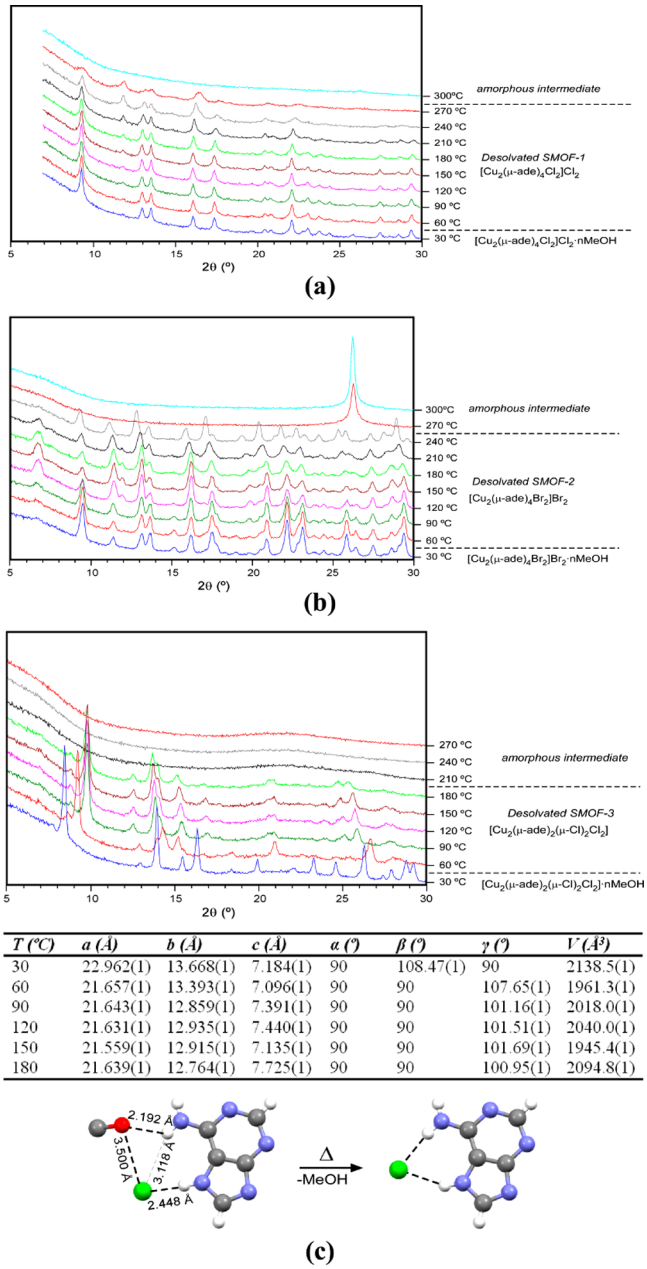

T (°C)	a (Å)	b (Å)	c (Å)	α (°)	β (°)	γ (°)	V (Å³)
30	22.962(1)	13.668(1)	7.184(1)	90	108.47(1)	90	2138.5(1)
60	21.657(1)	13.393(1)	7.096(1)	90	90	107.65(1)	1961.3(1)
90	21.643(1)	12.859(1)	7.391(1)	90	90	101.16(1)	2018.0(1)
120	21.631(1)	12.935(1)	7.440(1)	90	90	101.51(1)	2040.0(1)
150	21.559(1)	12.915(1)	7.135(1)	90	90	101.69(1)	1945.4(1)
180	21.639(1)	12.764(1)	7.725(1)	90	90	100.95(1)	2094.8(1)

Figure 4. Thermodiffractometric data of (a) **SMOF-1**, (b) **SMOF-2**, and (c) **SMOF-3**.

microscopy data on the fresh and outgassed samples allowed to rule out the presence of a substantial amount of impurities.

In a recent work Matzger and co-workers explained the discrepancies between crystallographic porosity and experimental gas uptake for Zn-HKUST-1 based on positron annihilation lifetime spectroscopy.[21] The authors state that the lack of gas uptake is due to the inherent surface instability after solvent removal which renders the material impermeable to molecular guests irrespective of the handling and activation methods used in the gas adsorption experiments. However, according to the latter work, the surface collapse is overcome when the sample is immersed in a solvent, and thus the porous network is well accessible.

Nonetheless, the present SMOFs have been shown to behave as an adsorbent when they were exposed to the vapors of methanol, acetone, dichloromethane, tetrachloromethane, and

dx.doi.org/10.1021/cg500634y | Cryst. Growth Des. 2014, 14, 4019−4029

water.[11] Thus, it seems that the above-described diffusion barrier resulting from the surface instability is not only overcome in solution but also when adsorbate molecules in the gas phase have enough interaction energy to pass through. In order to get further evidence on the latter statement herein we have carried gas adsorption measurements at higher temperatures by collecting the isotherms for CO_2 at 273 K and CH_4 at 298 K (Figure 5). Similarly to the previous

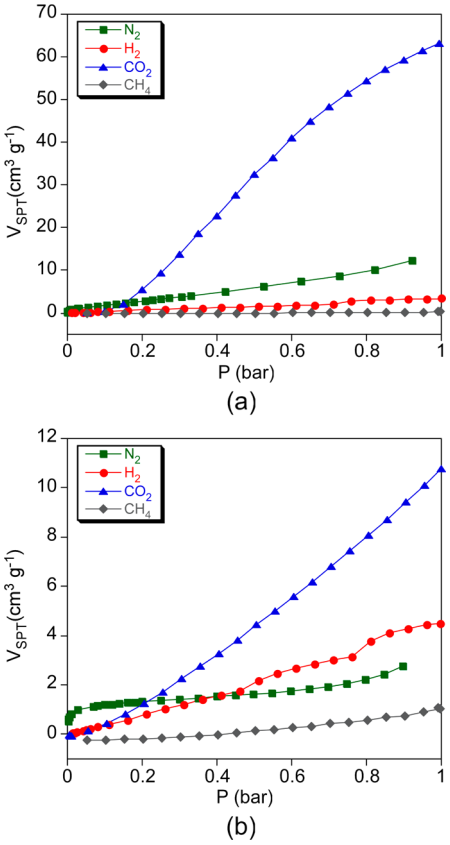

Figure 5. Adsorption isotherms for N_2 (77K), H_2 (77K), CO_2 (273 K), and CH_4 (298 K) for fresh samples of **SMOF-1** (a) and **-2** (b).

adsorbates methane adsorption is not observed. However, the CO_2 uptake shows a notable increase in both compounds. In fact while at pressures close to saturation, the N_2 uptake is 0.54 and 0.12 mmol/g for compounds **SMOF-1** and **-2**, and the CO_2 uptake increases about four times to reach values of 2.81 and 0.48 mmol/g, respectively. Considering the latter results this behavior can be rationalized on the basis of the thermal energy and of the polar nature of the adsorbate. The apolar CH_4 lacks of quadrupole moment, while CO_2 presents a relatively strong quadrupole moment (−0.8908 e·Å^2), sustantially greater than that for N_2 or H_2 (−0.2946 and +0.1288 e·Å^2, respectively).[22] Methane has not been able to permeate the surface although the increase of the adsorption temperature. Nonetheless, the higher measurement temperature and the stronger quadrupole moment of CO_2 confer the ability to diffuse through the surface barrier and permeate the porous network.

An additional proof that supports the hypothesis of the surface instability of these compounds is obtained from the gas adsorption study of the sample aging. In this regard, CO_2 measurements were carried out periodically during a month on samples of **SMOF-1** stored at room conditions (Figure 6a). It

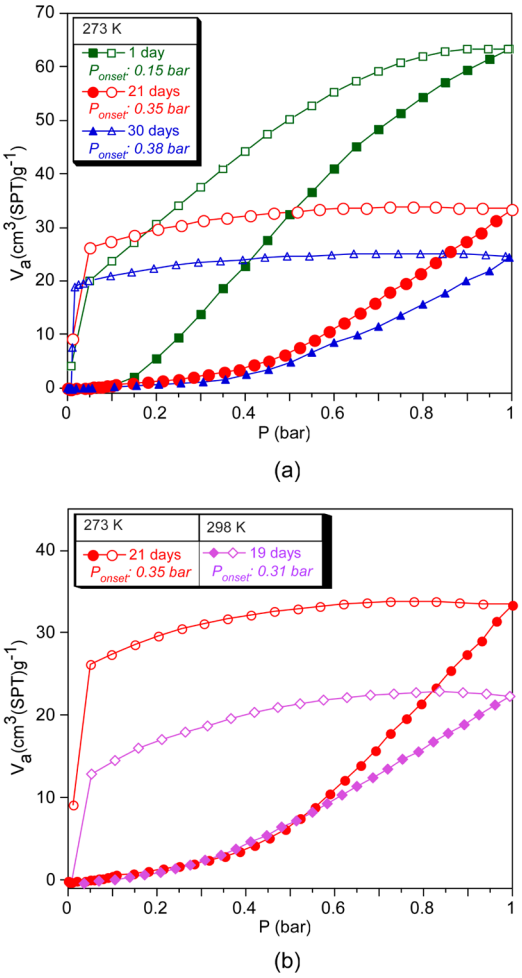

Figure 6. (a) CO_2 adsorption/desorption isotherms measured at 273 K showing the aging of **SMOF-1**. (b) CO_2 isotherms at 273 and 298 K. The onset pressure value is indicated for each case.

becomes clear that the CO_2 uptake capacity decreases progressively as the sample becomes older, and after a month the uptake at P = 1 bar is depleted in a ca. 60% when compared to its initial value (V_{STP} = 63.3 and 24.4 cm^{3}g^{-1} for the initial and one month aged sample). A second phenomenon related with the sample aging is the adsorption onset pressure calculated from the intersection between the tangents at the low pressure region and at the region of maximum slope of the adsorption branch (see Supporting Information). The adsorption of the initial sample shows a plateau with a negligible CO_2 uptake at pressures below 0.1 bar, and it requires a minimum breakthrough pressure (P_{onset}: 0.15 bar) to permeate the surface and reach the porous network. Moreover, the breakthrough pressure is shift to higher values as the sample gets older, to reach an onset value of P_{onset} = 0.38 bar for the sample aged during 1 month. This progressive increase of the breakthrough pressure is related with increase of the thickness of the collapsed surface which acts as a surface permeation barrier. Another feature that supports the presence of a surface barrier that hinders the diffusion of the molecules is related to the hysteresis cycle enclosed by desorption branch and its trend with the aging of the sample (Figure 6a). It is noteworthy that even though different equilibration times were used the hysteresis cycle was not affected, and as consequence, this hysteresis seems to be induced by structural features of the

dx.doi.org/10.1021/cg500634y | Cryst. Growth Des. 2014, 14, 4019−4029

sample. In fact, the hysteresis becomes more acute as the sample is aged, and its end-pressure is delayed also progressively (P_{end}: 0.05 and 0.02 bar for fresh and one month aged samples, respectively). This behavior is also congruent with an increasing thickness of the collapsed surface (or diffusion barrier) as the storage time goes on, which would also obstruct the release of the adsorbed molecules during the desorption process.

On the other hand, comparison between adsorption experiments carried out at 273 and 298 K samples similarly aged (Figure 6b) shows that the onset pressure (0.35 and 0.31 bar, respectively) is reduced with the increase of the experiment temperature, as the potential energy of the molecules to permeate the surface is increased.

In order to analyze the bulk crystal stability during CO_2 adsorption PXRD patterns where collected in a sample subjected to a CO_2 atmosphere with pressure ranging between 0.5 and 6 bar. Prior to the experiment the sample was outgassed at 150 °C during several hours. As it can be observed (Figure 7)

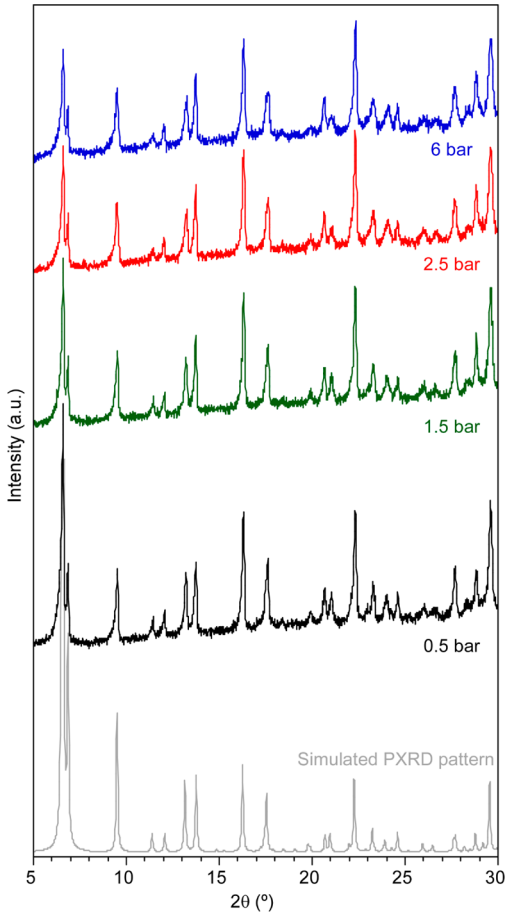

Figure 7. Comparison between experimental PXRD patterns collected at different CO_2 pressures and simulated PXRD pattern for the pristine crystal structure of **SMOF-1**.

all the experimental reflections match the ones corresponding to the simulated patterns of **SMOF-2**, and in any case no shift in 2θ positions is observed which stands for stability of the bulk crystallinity and for the bulk framework rigidity during the CO_2 adsorption process (i.e., reversible structural changes caused by CO_2 uptake can be disregarded, as for example, the so-called breathing effect).[23]

Regarding to the peak intensity, even though most of the peaks show no changes, the intensity of certain reflections is significantly affected. Figure 8a shows the trend of three

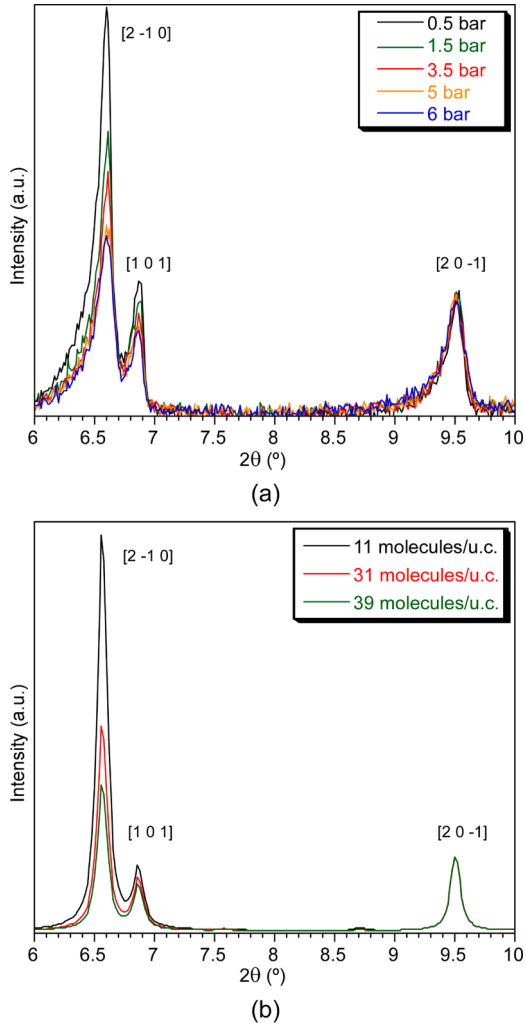

Figure 8. PXRD data for **SMOF-1** within 6−10°: (a) experimental patterns with increasing CO_2 pressure. (b) Simulated PXRD patterns from GCMC low energy configurations with increasing CO_2 uptake per unit cell.

reflections within the 6−10° 2θ range. As it can be observed [2 0 $\bar{1}$] reflection remains unvarying, while the intensity of [2 $\bar{1}$ 0] and [1 0 1] decays continuously with the increasing CO_2 pressure, which seems to be related to the CO_2 uptake within the structural pores. In order to confirm the latter proposal Grand Canonical Monte Carlo (GCMC) calculations were carried out in which the porous framework of **SMOF-1** was loaded with different amounts of CO_2 (see Supporting Information). Low energy configurations of the adsorbed molecules were used to model how the PXRD patterns are affected by the CO_2 (Figure 8b). The trend derived from the GCMC simulations matches the observed for experimental PXRD patterns, which allows us to state that intensity decay of the cited of reflections ([2 $\bar{1}$ 0] and [1 0 1]) is due the CO_2 presence within the 1D pores. When coordinates of CO_2 molecules are considered, no symmetry relation is found in any of the GCMC calculations. However, there is a periodicity of the preferential sites of adsorption (most sites derived from

dx.doi.org/10.1021/cg500634y | Cryst. Growth Des. 2014, 14, 4019−4029

probability density distribution for the center of mass of CO_2 molecule) in which electron density coming from adsorbed gas is accumulated (see Figure S5 in the Supporting Information). As a consequence, the decay of the mentioned reflections can be attributed to this periodically distributed averaged electron density of the adsorbed molecules.

Gas Adsorption Experiments of $[Cu_2(\mu\text{-adenine})_2(\mu\text{-Cl})_2(Cl)_2]\cdot 2MeOH$ (3, SMOF-3). In order to assess the stability of the unsolvated **SMOF-3** thermogravimetric and variable temperature PXRD experiments were carried out (see Supporting Information). Thermogravimetric analysis (TGA) shows that the solvent molecules are released easily at temperatures below 100 °C. Afterward the TGA curve shows a stability plateau that extends up to 245 °C. At higher temperatures the compound decomposes in successive steps to yield CuO as the final residue at temperatures above 475 °C. The thermodiffractometric measurements show a significant difference between the diffractogram performed at 30 °C and those performed between 90 and 180 °C (Figure 4c). The cell parameters indexed for the PXRD pattern collected at 30 °C match the ones corresponding to the single crystal structure. However, the PXRD pattern change observed at temperatures above 60 °C lead to new unit cell parameters closely related to the previous ones but with a significant change in the unit cell transforming it to a nonstandard monoclinic setting with $\gamma \neq 90°$, but maintaining the cell volume nearly constant. This transformation is related to a rearrangement of the synthon established between the Hoogsteen face and the chloride anion once the methanol molecule is released. All this indicates that although the supramolecular structure presents a moderate change its overall supramolecular crystal structure remains essentially stable up to 180 °C.

In order to assess the permanent porosity inferred from thermodiffractometric measurement we proceeded to measure gas adsorption isotherms on freshly synthesized sample of **SMOF-3** which was activated under a vacuum at 140 °C during 12 h to eliminate solvent guest molecules. The results and conclusions derived from the study of the gas adsorption behavior of **SMOF-1** and **SMOF-2** suggest that the surface weakeness of this kind of supramolecular compounds can make routine nitrogen adsorption isotherms not suitable for the study their porous features. In fact, **SMOF-3** presents a computed surface area of 361 $m^2\ g^{-1}$, but the experimental N_2 adsorption isotherm corresponds to a nonporous material. **SMOF-3** adsorbs a significant amount of CO_2 as depicted by Figure 9, but comparatively smaller than **SMOF-1** and **SMOF-2**, due to the greater free volume and surface area of the latter ones. Similarly to the precedent supramolecular microporous compounds, **SMOF-3** presents a breakthrough pressure close to P = 0.31 bar.

CONCLUSIONS

It becomes clear how a combination of rigid tectons with rigid synthons spreading at least in three noncoplanar directions is a well-suited route to obtain porous supramolecular networks. In this context, the metal-nucleobase complexes can be good candidates to fulfill both requirements when the nucleobase is anchored to the discrete entity by at least two positions. This anchorage and the aromatic nature of the nucleobase provide rigid supramolecular building units. On the other hand, the well-known complementary hydrogen bonding established between the nucleobases ensures the necessary rigidity of these synthons. Therefore, as it has been probed here the chances to obtain 3D supramolecular metal−organic frameworks based on metal-nucleobase systems are high. However, it is necessary to take care of the synthetic conditions in order to ensure the presence of the required direct hydrogen bonding interactions between the nucleobases. Related to this latter issue, the presence of water molecules can disrupt these direct adenine···adenine hydrogen bonding interactions, leading to nonporous materials as evidenced by the crystal structure of $[Cu_2(\mu\text{-adenine})_4Cl_2]Cl_2\cdot 8H_2O$.[24] The direct hydrogen bonding disrupting capacity of the water molecule seems also to be responsible of the surface instability observed in **SMOF-1**, **-2** and **-3**.

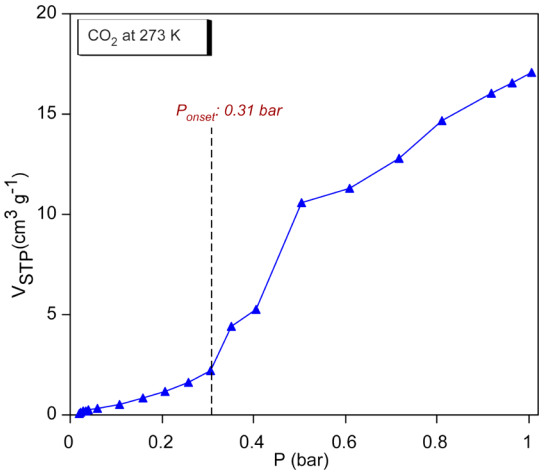

Figure 9. CO_2 adsorption isotherm **SMOF-3** at 273 K.

ASSOCIATED CONTENT

Supporting Information

Hydrogen bonding interaction tables, thermogravimetric measurements, thermodiffractometric analysis, onset pressure calculation on SMOFs, details on GCMC calculations, and cif files. This material is available free of charge via the Internet at http://pubs.acs.org.

AUTHOR INFORMATION

Corresponding Authors

*(G.B.) E-mail: garikoitz.beobide@ehu.es. Fax: (internat) +34-94601-3500.

*(O.C.) E-mail: oscar.castillo@ehu.es.

Author Contributions

#These authors (J.T.-G. and G.B.) contributed equally.

Notes

The authors declare no competing financial interest.

ACKNOWLEDGMENTS

Financial support from the Gobierno Vasco (IT477-10, SAIOTEK S-PE12UN004, SAIOTEK S-PE13UN016) and the Universidad del País Vasco/Euskal Herriko Unibertsitatea (UFI 11/53, postdoctoral fellowship) is gratefully acknowledged. Technical and human support provided by SGIker (UPV/EHU, MINECO, GV/EJ, ERDF and ESF) and by Mrs. Sandra Maracke from the University of Hamburg is also acknowledged.

REFERENCES

(1) (a) Lippert, B. *Coord. Chem. Rev.* **2000**, *200−202*, 487. (b) Lippert, B. In *Progress in Inorganic Chemistry*; Karlin, K. D., Ed.;

Wiley: New York, 2005; Vol. *54*, Chapter 6. (c) Sanz Miguel, P. J.; Amo-Ochoa, P.; Castillo, O.; Houlton, A.; Zamora, F. In *Metal Complex-DNA Interactions*; Hadjiliadis, N., Sletten, E., Eds.; Blackwell-Wiley: New York, 2009, Chapter 4. (d) Castillo, O.; Luque, A.; García-Terán, J. P.; Amo-Ochoa, P. In *Macromolecules Containing Metal and Metal-Like Elements*; Abd-El-Aziz, A. S., Carraher, Ch.E., Pittman, Ch.U., Zeldin, M., Eds.; Wiley, New York, 2009; Vol. *9*, Chapter 9. (e) Lippert, B. In *Nucleic Acid-Metal Ion Interactions*; Hud, N. V., Ed.; RSC Publishing, Cambridge,2009; Chapter 2. (f) Verma, S.; Mishra, A. K.; Kumar, J. *Acc. Chem. Res.* **2010**, *43*, 79. (g) Beobide, G.; Castillo, O.; Cepeda, J.; Luque, A.; Pérez-Yáñez, S.; Román, P.; Thomas-Gipson, J. *Coord. Chem. Rev.* **2013**, *257*, 2716.

(2) (a) En-Cui, Y.; Hong-Kun, Z.; Yan, F.; Xio-Jun, Z. *Inorg. Chem.* **2009**, *48*, 3511. (b) García-Terán, J. P.; Castillo, O.; Luque, A.; García-Couceiro, U.; Román, P.; Lloret, F. *Inorg. Chem.* **2004**, *43*, 5761.

(3) (a) Choquesillo-Lazarte, D.; Brandi-Blanco, M. P.; García-Santos, I.; González-Pérez, J. M.; Castiñeiras, A.; Niclos-Gutierrez, J. *Coord. Chem. Rev.* **2008**, *252*, 1241. (b) García-Terán, J. P.; Castillo, O.; Luque, A.; García-Couceiro, U.; Beobide, G.; Román, P. *Dalton Trans.* **2006**, 902.

(4) (a) Cepeda, J.; Castillo, O.; García-Terán, J. P.; Luque, A.; Pérez−Yáñez, S.; Roman, P. *Eur. J. Inorg. Chem.* **2009**, 2344. (b) Suggs, J. W.; Dube, M. J.; Nichols, M. *J. Chem. Soc., Chem. Commun.* **1993**, 307. (c) Wei, C. H.; Jacobson, K. B. *Inorg. Chem.* **1981**, *20*, 356. (d) Gagnon, C.; Hubert, J.; Rivest, R.; Beauchamp, A. L. *Inorg. Chem.* **1977**, *16*, 2469.

(5) (a) Terzis, A.; Beauchamp, A. L.; Rivest, R. *Inorg. Chem.* **1973**, *12*, 1166. (b) de Meester, P.; Skapski, A. C. *J. Chem. Soc. A* **1971**, 2167. (c) Mastropietro, T. F.; Armentano, D.; Marino, N.; De Munno, G. *Polyhedron* **2007**, *26*, 4945. (d) González-Pérez, J. M.; Alarcón-Payer, C.; Castiñeiras, A.; Pivetta, T.; Lezama, L.; Choquesillo-Lazarte, D.; Crisponi, G.; Niclós-Gutiérrez, J. *Inorg. Chem.* **2006**, *45*, 877. (e) Sletten, E. *Acta Crystallogr., Sect. B* **1969**, *25*, 1480. (f) Pérez-Yáñez, S.; Beobide, G.; Castillo, O.; Cepeda, J.; Luque, A.; Román, P. *Cryst. Growth Des.* **2012**, *12*, 3324.

(6) Amo-Ochoa, P.; Sanz-Miguel, P. J.; Castillo, O.; Sabat, M.; Lippert, B.; Zamora, F. *J. Biol. Inorg. Chem.* **2007**, *12*, 543.

(7) (a) Eddaoudi, M.; Moler, D. B.; Li, H. L.; Chen, B. L.; Reineke, T. M.; ÓKeeffe, M.; Yaghi, O. M. *Acc. Chem. Res.* **2001**, *34*, 319. (b) Yaghi, O. M.; ÓKeeffe, M.; Ockwig, N. W.; Chae, H. K.; Eddaoudi, M.; Kim, J. *Nature* **2003**, *423*, 705. (c) Kitagawa, S.; Kitaura, R.; Noro, S. *Angew. Chem., Int. Ed.* **2004**, *43*, 2334. (d) Perry, J. J.; Perman, J. A.; Zaworotko, M. J. *Chem. Soc. Rev.* **2009**, *38*, 1400.

(8) (a) Desiraju, G. R. In *Crystal Engineering: The Design of Organic Solids*; Elsevier: New York, 1989. (b) Etter, M. C. *Acc. Chem. Res.* **1990**, *23*, 120. (c) Etter, M. C. *J. Phys. Chem.* **1991**, *95*, 4601.

(9) Reger, D. L.; Debreczeni, A.; Smith, M. D.; Jezierska, J.; Ozarowski, A. *Inorg. Chem.* **2012**, *51*, 1068.

(10) Nugent, P. S.; Rhodus, V. L.; Pham, T.; Forrest, K.; Wojtas, L.; Space, B.; Zaworotko, M. J. *J. Am. Chem. Soc.* **2013**, *135*, 10950.

(11) Thomas-Gipson, J.; Beobide, G.; Castillo, O.; Cepeda, J.; Luque, A.; Pérez-Yáñez, S.; Aguayo, A. T.; Román, P. *CrystEngComm* **2011**, *13*, 3301.

(12) *CrysAlisPro*, version 1.171.35.15; Agilent Technologies, Yarnton, UK, 2011.

(13) Altomare, A.; Cascarano, M.; Giacovazzo, C.; Guagliardi, A. *J. Appl. Crystallogr.* **1993**, *26*, 343.

(14) Sheldrick, G. M. *SHELXL-97, Program for X-ray Crystal Structure Refinement*; University of Göttingen: Göttingen, Germany, 1997.

(15) Farrugia, L. J. *J. Appl. Crystallogr.* **1999**, *32*, 837.

(16) Van der Sluis, P.; Spek, A. L. *Acta Crystallogr.* **1990**, *A46*, 194.

(17) Spek, A. L. *Acta Crystallogr.* **1990**, *A46*, C34.

(18) (a) Pandey, M. D.; Mishra, A. K.; Chandrasekhar, V.; Verma, S. *Inorg. Chem.* **2010**, *49*, 2020. (b) Mishra, A. K.; Purohit, C. S.; Kumar, J.; Verma, S. *Inorg. Chim. Acta* **2009**, *362*, 855. (c) Beck, W. M.; Calabrese, J. C.; Kottmair, N. D. *Inorg. Chem.* **1979**, *18*, 176. (d) Sánchez-Moreno, M. J.; Choquesillo-Lazarte, D.; González-Pérez, J. M.; Carballo, R.; Castiñeiras, A.; Niclós-Gutiérrez, J. *Inorg. Chem. Commun.* **2002**, *5*, 800. (e) Pérez-Yáñez, S.; Castillo, O.; Cepeda, J.; García-Terán, J. P.; Luque, A.; Román, P. *Inorg. Chim. Acta* **2011**, *365*, 211. (f) An, J.; Fiorella, R. P.; Geib, S. J.; Rosi, N. L. *J. Am. Chem. Soc.* **2009**, *131*, 8401.

(19) Blatov, V. A.; TOPOS Main Page; **2006**, *7*, 4.

(20) Spek, A. L. *J. Appl. Crystallogr.* **2003**, *36*, 7.

(21) Feldblyum, J. I.; Liu, M.; Gidley, D. W.; Matzger, A. J. *J. Am. Chem. Soc.* **2011**, *133*, 18257.

(22) NIST Computational Chemistry Comparison and Benchmark Database NIST Standard Reference Database Number 101, Release 16a, , Johnson, R. D., III, Ed.; National Institute of Standards and Technology: Gaithersburg, MD , August 2013; http://cccbdb.nist.gov/.

(23) (a) Ramsahye, N. A.; Maurin, G.; Bourrelly, S.; Llewellyn, P. L.; Loiseau, T.; Serre, C.; Férey, G. *Chem. Commun.* **2007**, 3261. (b) Serre, C.; Bourrelly, S.; Vimont, A.; Ramsahye, N. A.; Maurin, G.; Llewellyn, P. L.; Daturi, M.; Filinchuk, Y.; Leynaud, O.; Barnes, P.; Férey, G. *Adv. Mater.* **2007**, *19*, 2246.

(24) de Meester, P.; Skapski, A. C. *J. Chem. Soc. A* **1971**, 2162.